



Integrative and multi-disciplinary framework for the 3D rehabilitation of large mandibular defects

Khaja Moiduddin¹ · Syed Hammad Mian¹ · Naveed Ahmed² · Wadea Ameen^{1,3} · Hisham Al-Khalefah¹ · Muneer khan Mohammed¹ · Usama Umer¹

Received: 17 July 2019 / Accepted: 26 November 2019 / Published online: 8 January 2020
© Springer-Verlag London Ltd., part of Springer Nature 2020

Abstract

The restoration of mandibular defects, especially large deformities is regarded as the most challenging surgical procedure owing to complicated anatomy and the requirement of customized design. Presently, the commercially available reconstruction plates with standard shapes and sizes are frequently utilized. However, these typical plates exhibit several disadvantages, including high cost, poor performance, etc. They are ineffective and do not exactly match the bone contours. Besides, trial and miss approach and several revisions associated with these plates involve significant effort and time. To overcome these issues, a framework based on the integration of design, analysis, evaluation, and fabrication phases have been developed and implemented. The objective was the attainment of a cost-effective, reliable, and sturdy design for the mandibular implant. A customized plate merged with a mesh structure matching the patient bone contours as well as guide and support the growth of neighboring bones was the crux of this mandible implant. The proposed methodology was made of three primary pillars: technology unification, multi-disciplinary notion, and a quality emphasis. A lattice structure, instead of a solid framework was utilized to reconstruct the large mandibular defect. Indeed, the various porous structures were analyzed to finally derive the appropriate lattice structure. The scans from computer tomography were utilized to model the customized plate and scaffold framework, while electron beam melting was used to fabricate the implant. Moreover, the proposed implant design was analyzed using finite element analysis as well as the fabricated specimen was validated for mechanical and structural behavior. The biomechanical analysis outcome revealed lower stresses (214.77 MPa) as well as well-connected structures involving proper porosity and robust mechanical properties. The cost analysis also established that the employment of the proposed design would result in a lesser burden on the patient as compared to the existing practices.

Keywords Customized implant · Additive manufacturing · Electron beam melting · Stress distribution · Lattice reconstruction plate · Mandibular restoration

Electronic supplementary material The online version of this article (<https://doi.org/10.1007/s00170-019-04762-3>) contains supplementary material, which is available to authorized users.

✉ Khaja Moiduddin
kmoiduddin@gmail.com; khussain1@ksu.edu.sa

Syed Hammad Mian
syedhammad68@yahoo.co.in

Naveed Ahmed
anaveed@ksu.edu.sa

Wadea Ameen
wadeaameen@gmail.com

Hisham Al-Khalefah
halkhalefah@ksu.edu.sa

Muneer khan Mohammed
muneerkm@ksu.edu.sa

Usama Umer
uummer@ksu.edu.sa

¹ Advanced Manufacturing Institute, King Saud University, Riyadh, Saudi Arabia

² Department of Industrial and Manufacturing Engineering, University of Engineering and Technology, Lahore, Pakistan

³ Industrial Engineering Department, College of Engineering, King Saud University, Riyadh, Saudi Arabia

1 Introduction

The large mandibular defect is complex and results in greater bone loss from the body of the patient. These defects are primarily caused by trauma, tumor resection, or infection [1]. They need immediate attention to restore the aesthetic features and functional performance of the mandible. Currently, the commercially available titanium reconstruction plates are being widely used to restore the mandibular defects. These commercial reconstruction plates come up in standard shapes and sizes. As a result, the surgeons have to spend a considerable amount of time matching the plate with the bone contours. It is because each patient possesses different bone anatomy and curvature, which disfavor the employment of standard plates without bending and twisting. Moreover, any mismatch between the reconstruction plate with bone contour results in implant failure, and its customization requires several revisions which lead to stress and discomfort to the patient.

The recent developments in data acquisition, image processing, computer-aided design (CAD), and advanced manufacturing processes have been instrumental in revolutionizing the medical industry, specially the customized implants business. These innovations can design and fabricate tailor-made implants to achieve higher customer satisfaction. The combination of lattice (mesh) structure and the solid plate are being widely employed to repair large bone defects in orthopedic applications [2]. Certainly, additive manufacturing has reformed the restorative industry through its ability to produce complex freeform geometrical structures effectively [3, 4]. It has been identified as an efficient manufacturing process with shorter lead time and lesser wastage as compared to other traditional manufacturing processes such as casting, forming (extrusion), and subtracting (machining) [5]. Among the many additive processes, the electron beam melting (EBM) has been regarded as a fast and successful method in the fabrication of custom-designed metallic implants with a Food and Drug Administration (FDA) and Conformité Européenne (CE) approval [6]. The lattice structure attached to the solid plate is valuable because it provides adhesion between the bone-implant interface, thus resulting in faster healing time and effective biological fixation. Indeed, several studies have pointed out that lattice geometry with well-interconnected pore is a promising alternative to the bulk geometry [7, 8]. The contemporary studies have identified EBM as a breakthrough in the fabrication of lattice structures with controlled porosity [9, 10]. Although the conventional techniques, including casting, powder metallurgy, and fiber deposition, had also been considered in the fabrication of lattice structure, they did not provide satisfactory outcomes [11, 12]. It is because these techniques yielded incompetent mesh structures with non-uniform porosity, impurities, and loose connection between them.

The reconstruction of large mandibular defects has been a complex task due to the unavailability of an effective and reliable methodology. Moreover, the current practice of employing commercially available standard plates is an expensive and inefficient approach. As a result, a rational and efficient methodology is developed to design and fabricate a customized mandibular implant. A custom-made implant unified with the lattice structure has been acquired through the fusion of computed tomography (CT) and additive manufacturing. A customized lattice reconstruction plate has been designed using the patient's CT scan images. To understand the mechanical behavior and stress–strain distribution of the designed lattice plate under the mastication (chewing) process, a three-dimensional (3D) finite element model (FEM) of the mandible and lattice plate was modeled and analyzed. Subsequently, the 3D printing technologies based on ARCAM's EBM (Möln dal, Sweden) were used for the fabrication of the titanium (Ti6Al4V ELI) lattice reconstruction plate. Ti6Al4V ELI (extra-low interstitial) is a high-purity titanium alloy with a reduced amount of O, N, C, and Fe, exhibiting improved ductility and toughness compared to standard grade 5 titanium alloy (Ti6Al4V) [13]. Furthermore, the energy dispersive X-ray spectroscopy (EDS), scanning electron microscopy (SEM), and micro-CT (μ -CT) tests were performed to evaluate the fabricated titanium lattice plate. Indeed, the objective of this study is to present a novel design approach for repairing large mandibular defects that can restore the best possible masticatory function and maintain facial aesthetics with fast healing. This research study has focused on automating the process of retrieving the customized lattice implant for the large mandibular defect. The novelty in the current study is threefold. First is the seamless integration of the various phases to restore the large mandibular defect. The adopted approach consisted of technology consolidation, simultaneous interdisciplinary association (engineering design, medical, manufacturing, quality fields, etc.), and a robust quality (mechanical, structural, and biomechanical analysis) strategy. Second, a large mandibular defect has been considered in this work. While a number of similar works have been published lately, they have primarily focused on the small and medium defect regions. A lattice structure, instead of a solid framework has been utilized to restore the large mandibular defect. The different porous structures were studied to finally come up with the most appropriate design. Third, quality by design policy was ensured so that the customized mandibular implant could be designed and fabricated properly from the outset without any defect. An exhaustive cost analysis has also been performed to establish that the adopted approach of realizing the customized reconstruction plates for large mandibular defects is economical.

2 Experimental methodology

The experimental methodology adopted to design and fabricate a customized, cost-effective mandibular implant was based on five modules as shown in Fig. 1. The various modules comprised of the design module, analysis (or simulation) module, fabrication module, evaluation module, as well as the cost analysis, to study the economics of the design and the suggested methodology.

The design module consisted of the following main sub-stages. The CT images acquired for the patient were processed, and the customized implant was designed. It also included the selection of an appropriate lattice structure for the mandibular implant. The design activities were primarily performed in an image processing software Mimics^R 17.0 (Materialise, Leuven, Belgium) [14]. Subsequently, the customized implant design obtained at the design stage was analyzed (or simulated) in ANSYS^R (Ansys Inc., Pennsylvania, USA) [15] to study the mechanical viability under various loading and chewing conditions. The customized implant design was then realized through fabrication using EBM. To assess the performance of the fabricated specimen, different tests, including powder metallurgical study, mechanical study, and structural characterization of the internal and external lattice structure was carried out. These evaluation studies were useful in finding the metallurgical bonding and strength between each layer of the lattice structure. The cost analysis was also required to ensure that the adopted methodology was reasonable as well as to comprehend that the customized implant was not expensive. This methodology is different owing to technology integration, interdisciplinary cooperation, and its goal of continuous customer satisfaction.

2.1 Design module

The methodology used in the design of a customized lattice reconstruction implant is illustrated in Fig. 2. This methodology was employed to achieve the unification of the various design, fabrication, and validation phases which can restore the large mandibular defect. It is different owing to its technology integration, interdisciplinary cooperation, and the goal of continuous customer satisfaction.

A patient suffering from a large mandibular defect was scanned (Fig. 2(a)) with a GE Light Speed VCT XTe scanner [16]. The scanned images in two-dimensional (2D) format (Fig. 2(b)) were stored in a database (Fig. 2(c)) as Digital Imaging and Communication in Medicine (DICOM) files which is the standard data format for storing medical images. Mimics[®] was used to import and process the 2D cross-sectional anatomical data (CT scan images) as well as to convert them into an accurate 3D model as shown in Fig. 2(d). The Hounsfield Unit (HU) which makes up the grayscale in medical CT scans, was adjusted in Mimics[®] to segregate the hard and soft tissues. Moreover, the region growing methods based on segmentation was employed to remove the undesired data (Fig. 2(e,f)) and partition the 3D model into different regions. The separation of masks and thresholding units were used to construct the compact (cortical) and trabecular (cancellous) bone using CT images. The region of interest “mandible” as shown in Fig. 2(g) was obtained after segmentation and saved as Standard Tessellation Language (STL) file for the implant design.

The successful reconstruction of implant depends on the implant design, its material, fixation, and of course, the skills

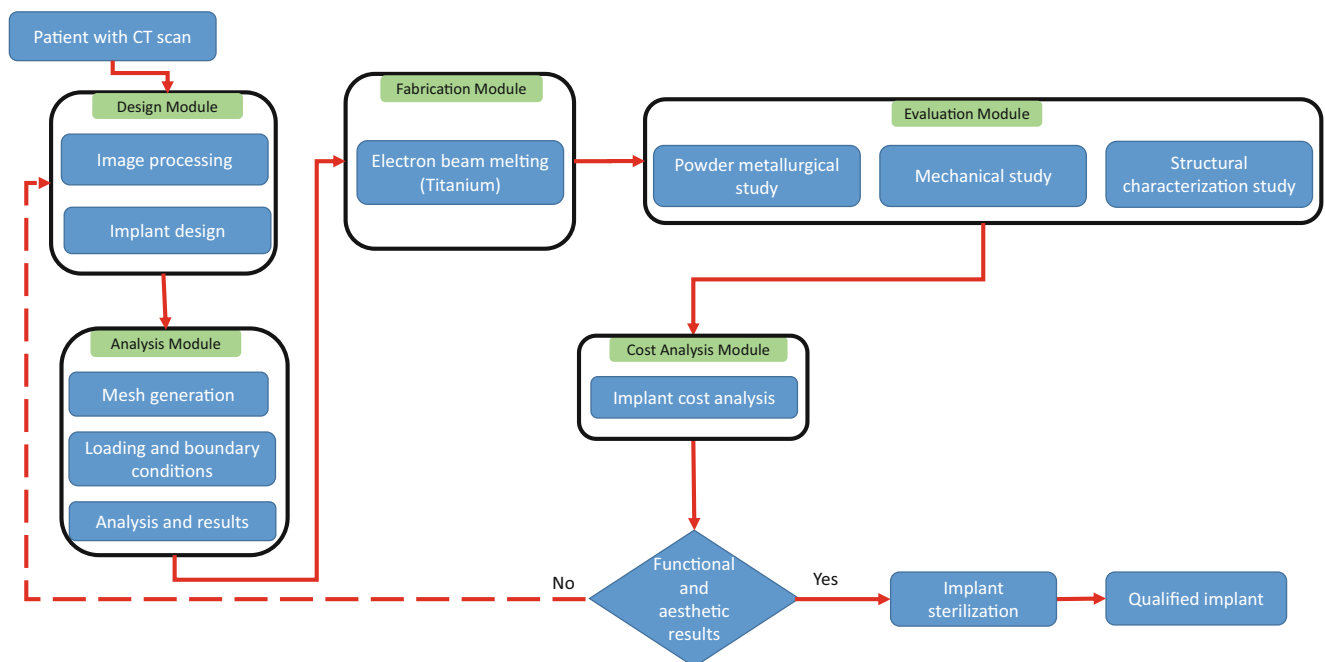


Fig. 1 Experimental methodology for the reconstruction of a customized implant

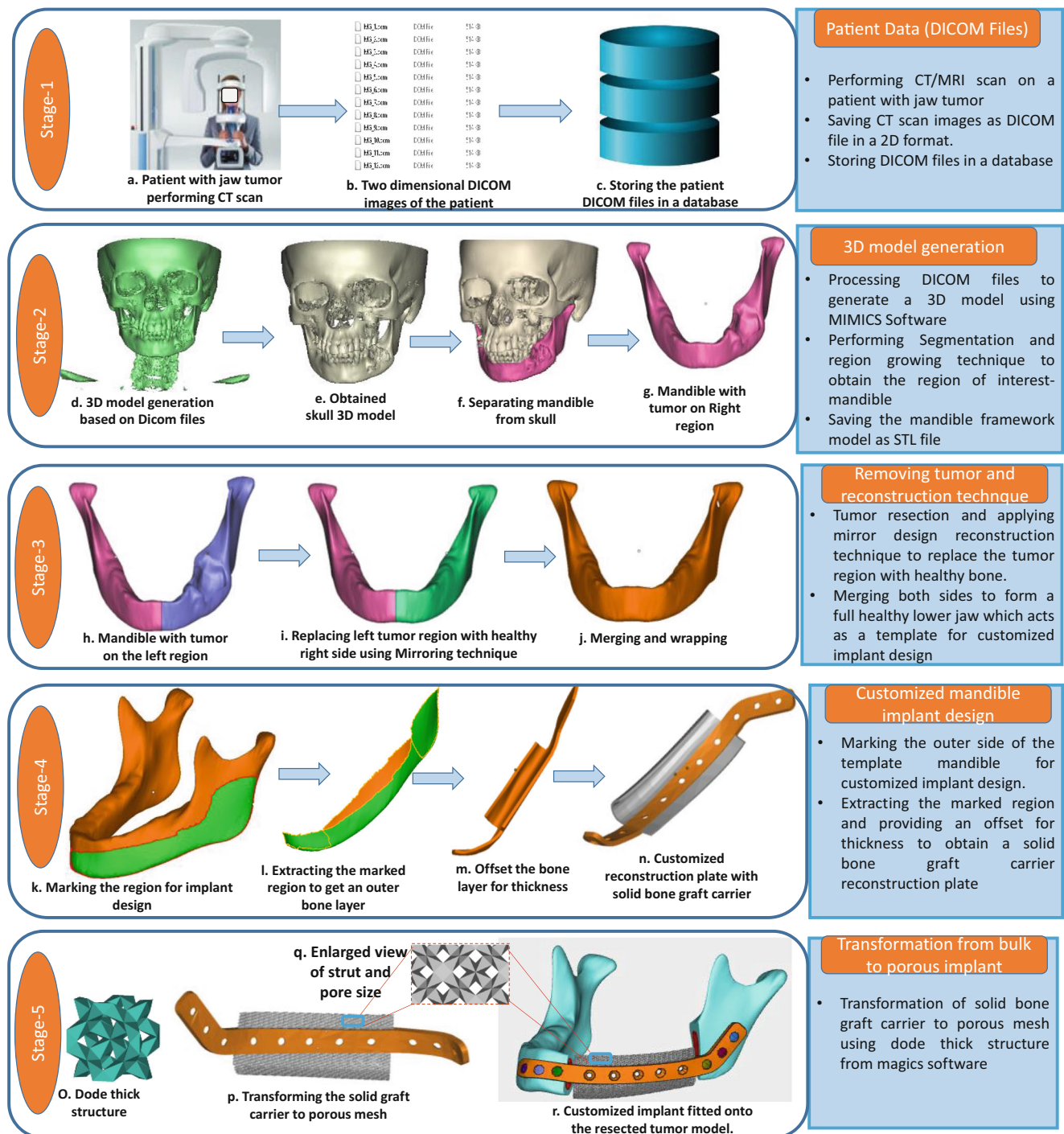


Fig. 2 The schematic process flow for the customized mandibular lattice reconstruction implant

of the surgeon [17]. There are several customized design techniques, but choosing the right technique which can provide better accuracy and the minimum deviation between the implant and bone contours is of utmost importance. Mirroring is one of the widely used image reconstruction techniques in cranial and maxillofacial applications [18, 19]. Therefore, the mirror image reconstruction technique (Fig. 2(h)) was employed in the customized mandibular implant design where

the left defective region was replaced by the healthy right side (Fig. 2(i)). Consequently, the merging and wrapping operations were performed to remove the gaps in the model as shown in Fig. 2(j). A smooth outer region was selected (Fig. 2(k)) and extracted on the mandibular model (Fig. 2(l)) which acts as a template for customized implant design. An offset thickness and taper screw holes were provided for implant fixation and stability as shown in Fig. 2(m). The bottom and

top thick (silver color) region of the mandibular implant was converted from solid (Fig. 2(n)) to lattice region using dode thick structure (Fig. 2(o)) by Magics® 18.0 (Materialise, Leuven, Belgium) as shown in Fig. 2(p). The designed mandibular implant with lattice structure was fitted onto the tumor-resected mandibular model as shown in Fig. 2(r). One of the advantages of having the lattice region (dode structure) is to use the attached mesh as a graft carrier with the customized implant. Several studies have reported dode structures to develop bone implants [20, 21]. Cansizoglu et al. [22] in his study have fabricated one lattice structure (hexagonal) and studied its effect on various cell dimensions. Horn et al. [23] have also investigated one-unit cell geometry (rhombic dodecahedron) with different unit cells and relative densities. In this study, the dode thick structure with different unit cell dimensions has been investigated. Consequently, the dode thick structure was evaluated in contrast to other structures as well. The purpose was to analyze the effect of different unit cell geometries and different structures on the patient-specific implant for biomedical application.

A consensus in the prior studies indicates that for optimal cell tissue growth, interconnected porosity of 50 to 80% and pore sizes ranging from 50 to 800 μm are desirable [24, 25]. Earlier studies have confirmed that the minimal pore size required for bone ingrowth is in the order of 50–100 μm whereas larger pore size initiates greater bone formation but on the other hand, affects the mechanical properties [26]. Markhoff et al. [27] studied different 3D titanium porous scaffolds and suggested that smaller pores of 400–620 μm and high porosity of 75% provide the highest implant–bone adhesion and

metabolic cell activity. In this study, three different unit cell sizes of 1, 2, and 3 mm of dode thick structure with a pore diameter of 220, 480, and 650 μm and a porosity level of 75% were designed as bone graft carrier as shown in Fig. 3. Based on the design, the unit cell 3 mm was found to contain gaps and discontinuity between the junctions which could lead to cracks and weak joints upon loading. The unit cells 1 and 2 mm found to show good inter-connections among the joints in the designed part. Upon further investigation, after EBM fabrication, it was revealed that the 1-mm unit cell contained trapped powder. This was due to small pore size which failed to remove the trapped powder after several attempts of blasting in the powder recovery system (PRS). Finally, the 2-mm unit cell was selected after the successful removal of the trapped powder.

In addition to different unit cell sizes, various dode structure of dode thin and dode medium from Materialise Magics® were evaluated [28]. These structures are different from each other based on their strut and pore sizes. As shown in Fig. 4, it was clear that the dode thick structure was interconnected through a good network of channels without any voids and gaps in comparison to dode medium and dode thin. Based on the above observation and evaluation, the dode thick 2-mm unit cell was selected for graft carrier.

The virtual assembly of the mandibular framework model comprising of compact and trabecular bones of the mandibular framework model with lattice (dode thick 2 mm) reconstruction plate and three condyle and chin screws was performed for fitting evaluation as shown in Fig. 5(a). This was achieved using Magics®. If there was an error in the design

Fig. 3 Evaluation of three different unit cell of dode thick structure

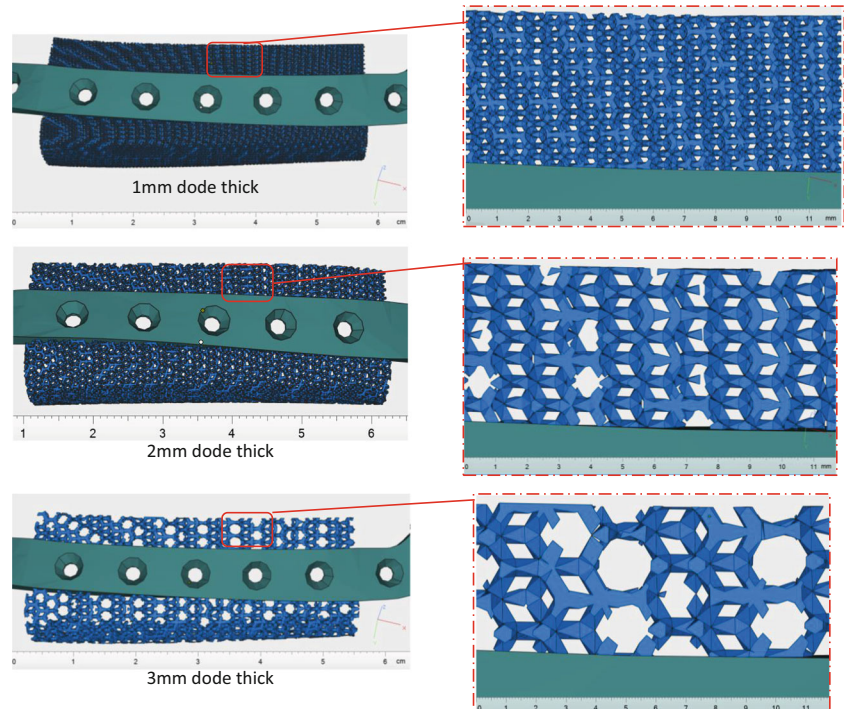


Fig. 4 Mandibular lattice implant with dode thin, dode medium, and dode thick lattice structure

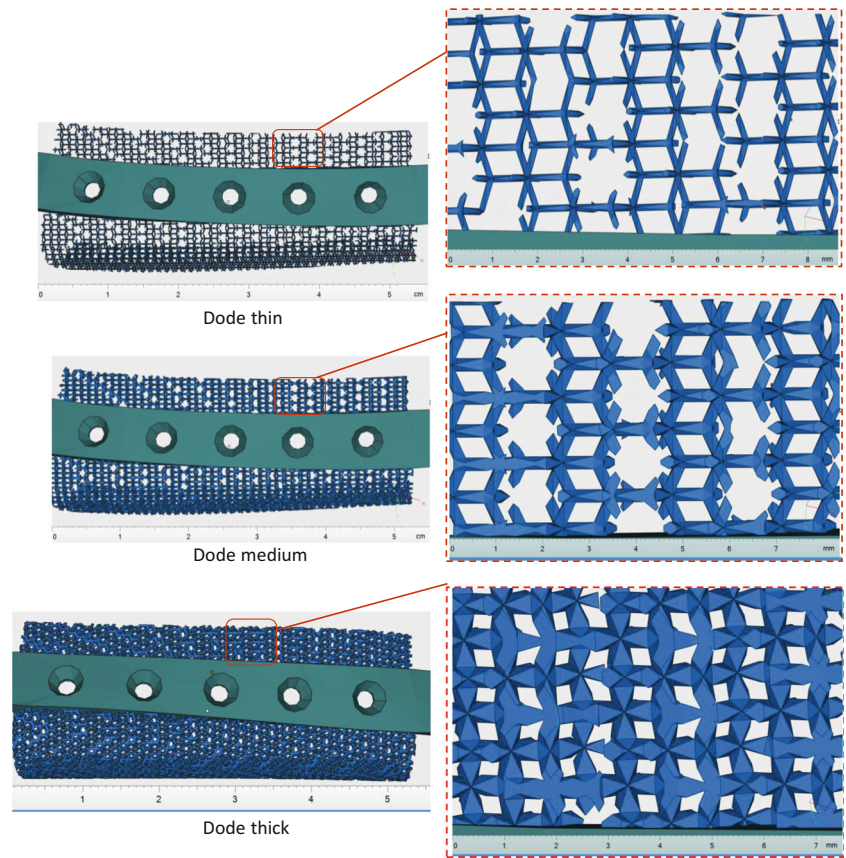


Fig. 5 **a** Virtual assembly of the lattice reconstruction plate, mandibular framework model and six bicortical screws, **b** sectional screw interface with compact and trabecular bone, and **c** close-up view of the countersink screw hole and the screws

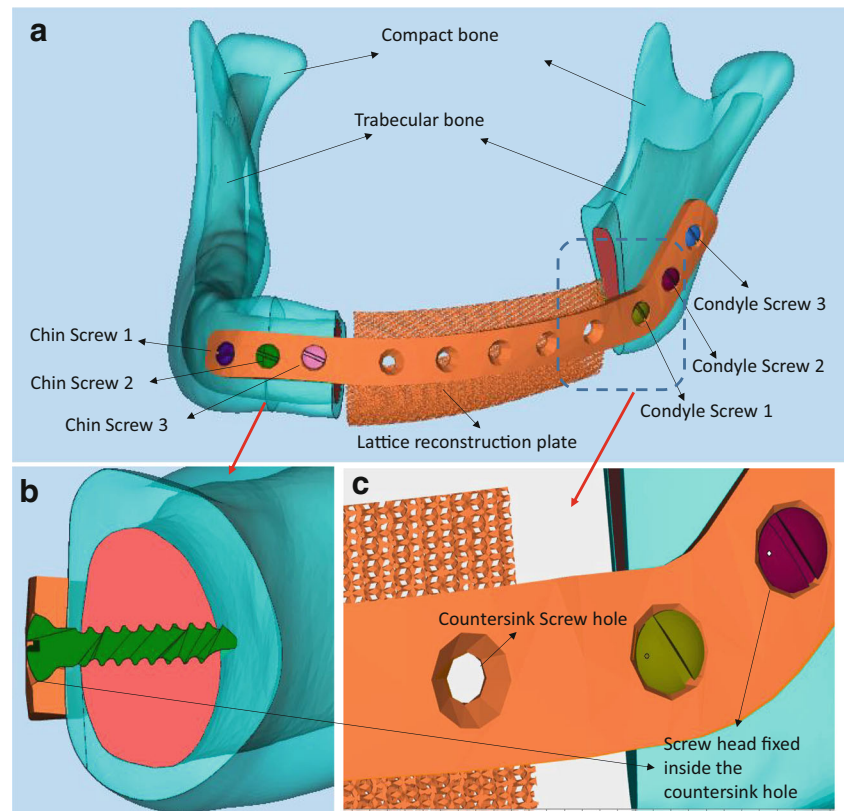


Table 1 Mechanical characteristics of study materials used in the FE model, [31, 32]

Materials	Young's modulus (MPa)	Poisson's ratio	Yield strength (MPa)
Compact bone	13,700	0.3	122
Trabecular bone	1370	0.3	2
Lattice reconstruction plate, (Ti6Al4V ELI)	120,000	0.3	930

assembly such as space and voids in-between the reconstruction plate and the framework model, the implant design process had to be repeated until the satisfactory results were achieved. The virtual assembly also helped in the intraoperative surgery and provided surgical guidelines to the surgeons in precision drilling and placement of the screws. The reconstruction plate was incorporated with countersink screw holes as shown in Fig. 5(b, c) so that the screw head passed completely inside the screw hole thus enhancing the patient comfort level and increasing the life of the implant. The mandible framework model with lattice reconstruction plate and screws were saved as Standard for the Exchange of Product (STEP) file for simulation.

2.2 Simulation module

The finite element analysis (FEA) was utilized to predict and refine the design before fabrication. It has been regarded as one of the most reliable simulation tools in bio-engineering

Table 2 Load magnitude and functional direction of masticatory muscles in Newton's (N) [36]

Masticatory muscles	X (N)	Y (N)	Z (N)
Masseter	50	-50	200
Medial pterygoid	0	-50	100
Temporalis	0	100	200

studies for determining the biomechanical phenomena under various loading conditions [29, 30]. The FEA software, Ansys® (ANSYS Inc., PA, USA), was used in this study to predict the mechanical behavior of the mandible reconstruction plate under the mastication process. The STEP file of the mandibular framework model was imported into Ansys®, and the material properties, meshes, and loading conditions were assigned. The mechanical characteristics of compact bone, trabecular bone, and plating system were considered as isotropic, homogenous, and linear elastic and this data was taken from literature studies (Table 1) [31, 32]. However, the bone mechanical properties were not considered linear elastic as the geometry, as well as material properties, changes from one person to another as per the age and sex [33, 34].

Before importing the mandibular model in Ansys®, customized patches were constructed which helped in defining the loading and boundary conditions efficiently as illustrated in Fig. 6(a).

To describe the loading on the mandibular model during the mastication process, three muscle forces temporalis, medial pterygoid, and masseter were included in the FEA study. These three muscle forces were simulated on the mandibular

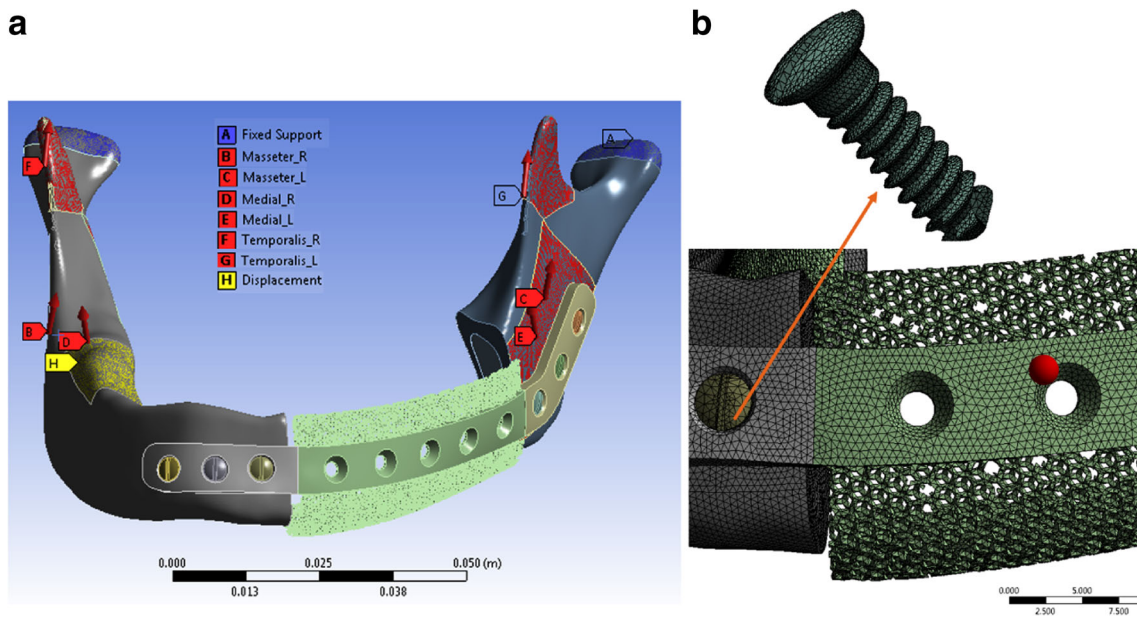


Fig. 6 a Details of loads and constraints on mandibular framework model with a lattice reconstruction plate and b global view of meshing on mandibular framework model

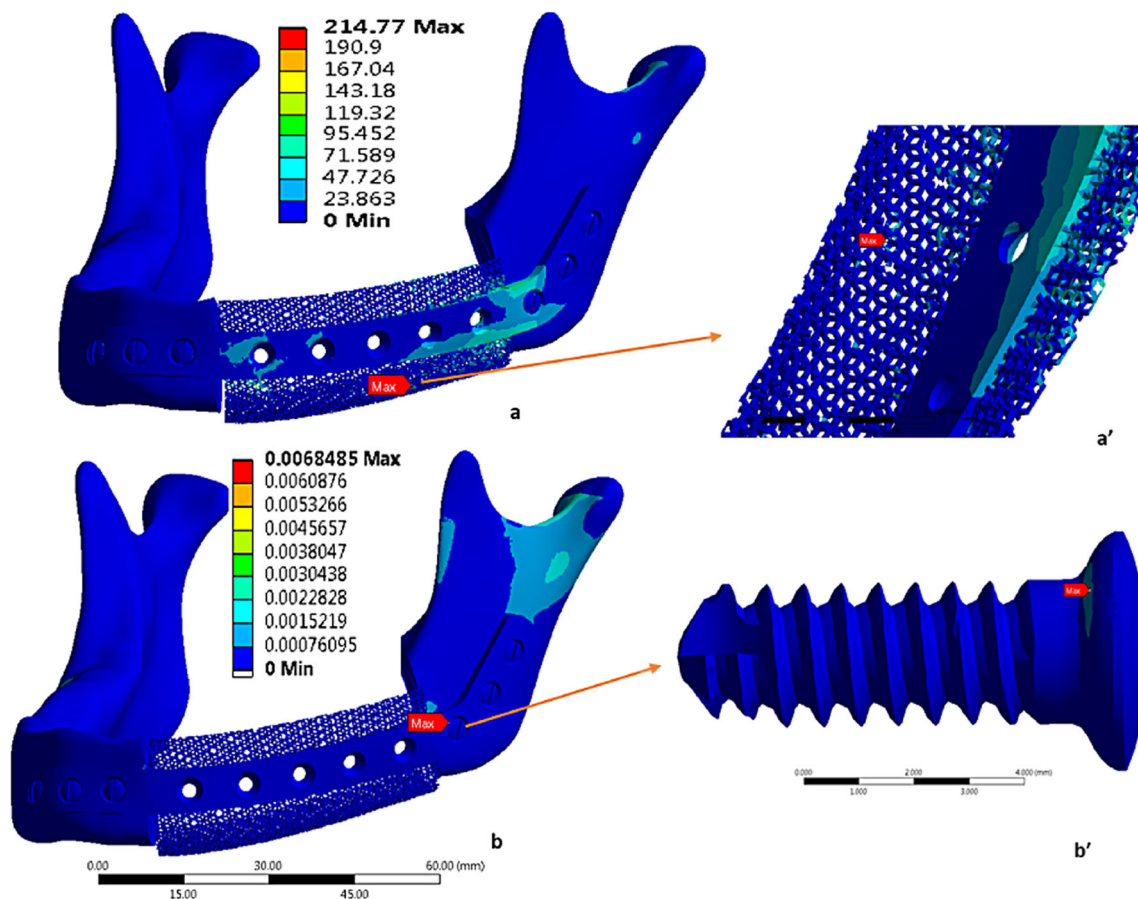


Fig. 7 (a) Stress distribution (Von Mises; MPa) of the mandible model, (a') enlarged view exhibiting max stress (MPa) on the lattice, (b) Strain distribution of the mandibular model, and (b') enlarged view of the screw illustrating max strain

framework model based on the discussion of clinicians and through a literature study [35]. The moment of chewing was simulated in the FEM with muscular forces and force vectors were taken in Newton (N) measurement unit as shown in Table 2. The muscular forces exerted by each muscle along the direction are shown in Fig. 6(a). The magnitude of each muscular force applied during mastication was derived from a previously published study [36]. The plate–bone and screw–bone interfaces meshed with 3D tetrahedral 10-node elements with the program control surface mesher are illustrated in Fig. 6(b). The connections between the interfaces were assumed as bonded based on literature studies [37, 38]. The loading records for the above FEM was implemented in Ansys® under

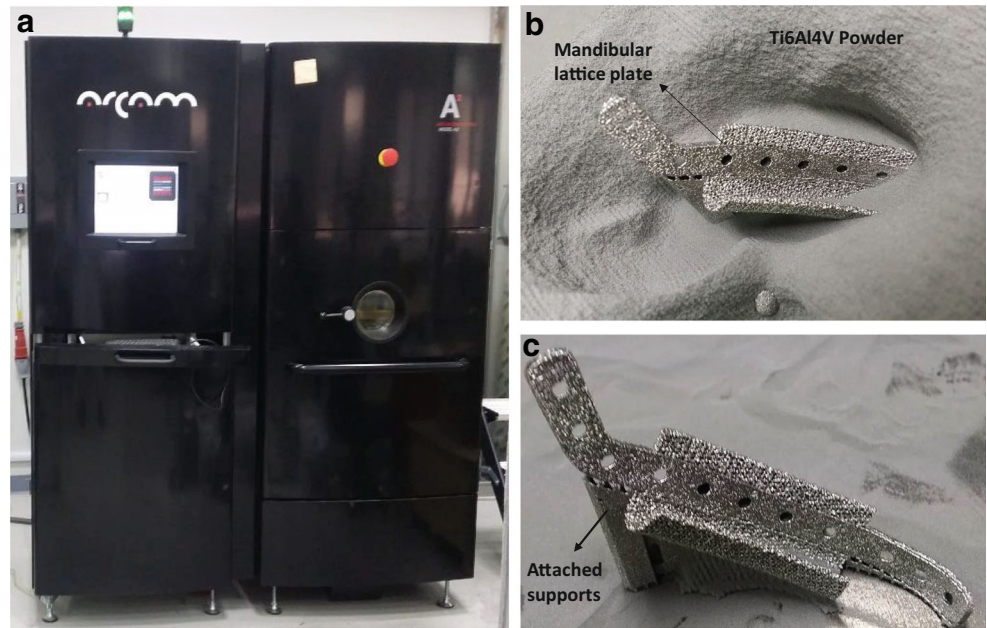
static load conditions. Under mastication, the superior part of both the condyles was kept fixed in all three axes. The vertical displacement was constrained at the right side of the mandible molar region to simulate the biting conditions. The molar region underwent near-zero displacements with axial chewing forces. This restraint movement acted perpendicular to the occlusal plane (Z direction) and conceded displacement freedom in the horizontal plane (X and Y direction) as illustrated in Fig. 6(a).

Note that it was difficult to simulate a complex geometrical model of the mandible when exposed to three muscular forces. The FEA provided an approximate solution for the lattice reconstruction plate attached to the mandibular framework

Table 3 Summary of FEA results under chewing conditions

Designed implant	Max Von Mises stress (MPa)	Max strain	Stress on first chin screw (MPa)	Stress on second chin screw (MPa)	Stress on third chin screw (MPa)	Stress on first condyle screw (MPa)	Stress on second condyle screw (MPa)	Stress on third condyle screw (MPa)
Lattice reconstruction plate	214.77	0.00684	61.85	39.76	53.61	127.71	125.07	84.44

Fig. 8 **a** ARCAM machine, **b** Semi-sintered (Ti6Al4V ELI) powder around the reconstruction plate, and **c** EBM reconstructed lattice plate with supports



model. Although several biomechanical studies have been performed on the mandibular reconstruction plates [35, 39], very few studies are available on the lattice reconstruction plate on the mandibular model. One of the main reasons is the complex nature of the lattice structure. The FEA results of the lattice reconstruction plate as shown in Fig. 7(a) predicted that the maximum Von Mises stresses were confined in the lattice region which was perceptible due to its low cross-sectional area.

The reconstruction plate was assumed to fail in case the Von Mises stresses exceeded the implant material yield strength. The maximum Von Mises stresses observed in the lattice reconstruction plate (214.77 MPa) and screws (127.71 MPa) were well below the yield point (800 MPa) of the titanium (Ti-6Al-4 V ELI) material. To further evaluate its flexibility, the FEM was accessed by observing the strains under chewing conditions. The maximum strain (Fig. 7(b)) found on the first condyle screw was of few microns (6.8 μm) thus reducing the chances of screw loosening. The

FEM was contemplated to be more steady and fixed when the bicortical screws hold the reconstruction plate intact [40, 41]. Hence, the plate which generates lower strains is considered more flexible and stable [39]. The simulation results of stress and strain distribution of the mandibular framework model assembly are presented in Table 3. On further observation of analysis results, it was found that the stresses were transmitted from the lower mandible (chin region) towards the upper mandible region (Condyle) thus satisfying the maxillofacial conditions during mastication [42].

2.3 Fabrication module

Upon successful completion of the analysis of the customized lattice reconstruction plate, the implant fabrication was carried out. Titanium alloy (Ti6Al4V ELI) was used for the fabrication of customized lattice reconstruction plates using EBM technology.

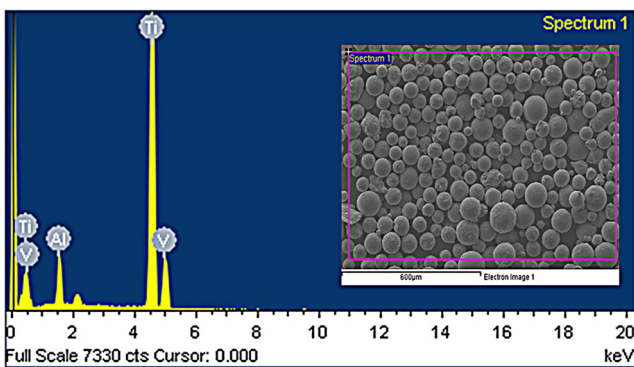


Fig. 9 Chemical composition of the used Ti6Al4V ELI powder (EDS test)

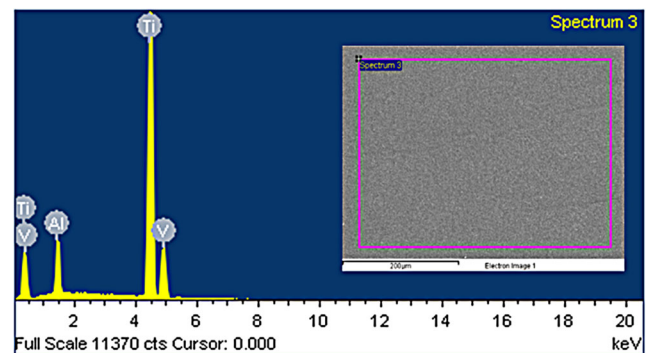


Fig. 10 EDS spectrum of fabricated plate

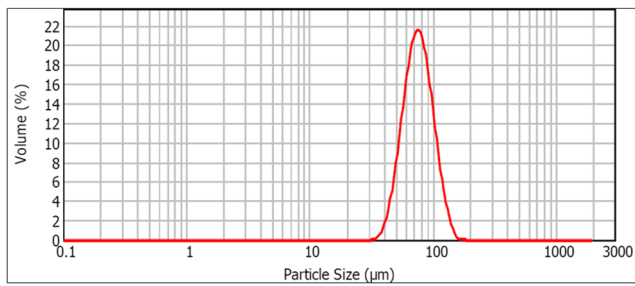


Fig. 11 Powder particle size distribution (laser diffraction technique)

Initially, the STL file of the lattice reconstruction plate was imported into Magics® for the optimization of triangular meshes and generation of support structures. The common STL errors such as gaps, bad contours, noise shells, overlapping and intersecting triangles, etc., were removed before generating support structures. The support structures play a vital role in the successful fabrication of 3D printed parts. Therefore, support structures were added to prevent the distortion and collapsing of parts during the build. The implant model (reconstruction plate) along with support structures were imported into ARCAM's build assembler software to convert the 3D STL geometry into thin slices of 2D cross-section (layers) and saved as EBM machine-readable ABF file. This ABF file contained all the instructions needed for the EBM machine control program to build the part in a layer-by-layer form. The EBM A2 machine as shown in Fig. 8(a) read the 2D cross-sectional layers and generated the beam of electrons to melt the part as per the geometry. The ARCAM's EBM builds parameters of the sintering and melting process were left unchanged along with the standard parameters of the 50- μm -layer thickness during fabrication.

For EBM fabrication, a sequence of three steps was performed for each built layer, consisting of distribution of powder evenly around the build plate, preheating and melting of the powder, and lowering the build platform to one-layer thickness (50 μm). This sequence of steps was repeated until the final part was built. The EBM-built

fabricated plate was then subjected to a PRS for blasting away the semi-sintered powder around the build plate as shown in Fig. 8(b). The blasting was done with the mixture of the same material (Ti6Al4V ELI) and air with high pressure of 6 bar to preserve its purity [43]. The blasted powder was sieved and refilled into the machine with fresh powder for the next build. The support structures as shown in Fig. 8(c) were added to assist the overhang parts and to dissipate the heat during the printing process thus preventing residual stresses. The attached supports were easily removed manually using simple tools such as plyer.

2.4 Evaluation module

The different verification tests were performed in this phase to validate the effectiveness of the acquired implant design. For example, the EDS (Oxford instruments, PLC, UK) equipped with SEM was conducted for titanium alloy before and after the fabrication of the reconstruction plate to evaluate its chemical composition. The EDS test for the Ti6Al4V ELI powder is illustrated in Fig. 9.

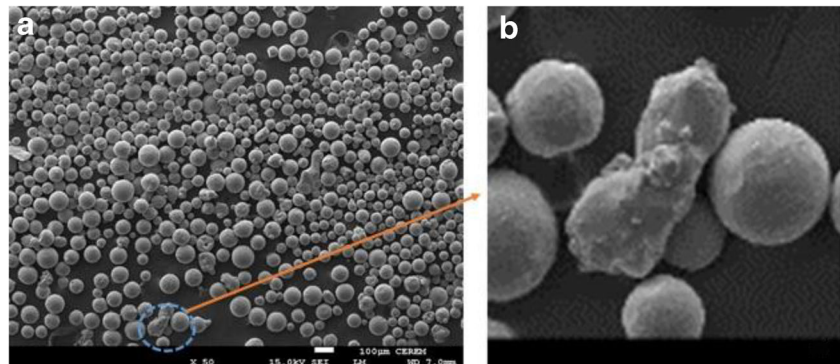
The chemical composition of the EBM specimen examined by the EDS test on post fabrication is shown in Fig. 10.

The powder particle size and shape influences the EBM build platform and the sintering kinetics between the particles. Hence, laser diffraction analysis was performed on feedstock powder (Ti6Al4V ELI) to measure the geometrical dimension as shown in Fig. 11.

The SEM analysis was conducted as shown in Fig. 12(a) to study the powder particle size morphology. It was observed that some of the spherical powder particles were in adhesion with other particles as shown in Fig. 12(b).

The structural characterization of the reconstruction plate was assessed depending on the external and internal pore structure. The open and interconnected lattice networks are essential for cell nutrition, proliferation, tissue migration, and vascularization and formation of new tissues [44]. Besides, there should be good interconnections between struts without any cracks or defects. The pore diameter and strut size

Fig. 12 **a** SEM micrograph of Ti6Al4V ELI powder and **b** enlarged view of two adhesion particles



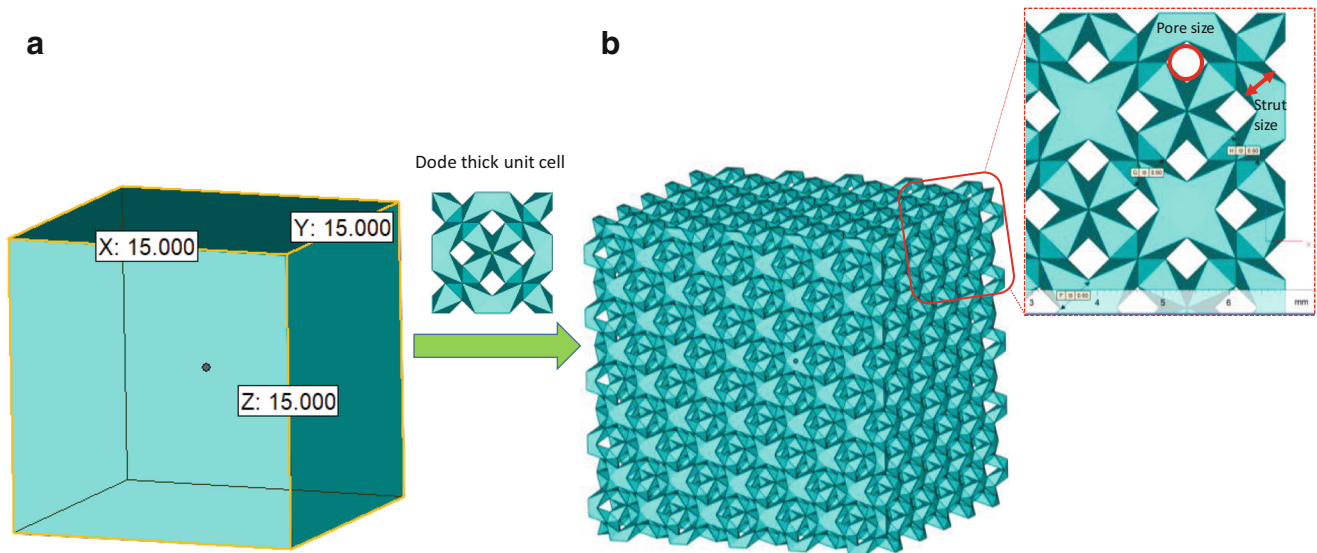


Fig. 13 Transformation of a solid cube to dodecahedral lattice structure and its measurement of strut thickness and pore diameter

are important characteristics of a lattice material because the properties of the lattice material depend on the pore size, strut/wall size, and shape [45]. Hence, a solid cube of $15 \times 15 \text{ mm}^2$ (Fig. 13(a)) was designed and transformed into a dodecahedral lattice structure of 2 mm unit cell (Fig. 13(b)) and its internal, as well as external pore structure, was studied. The optical microscope (Motic® BA310, Hong Kong) was utilized to estimate the pore and strut size of the EBM-produced lattice cubes. It was indeed performed to test the difference between the design and EBM-fabricated parts.

Figure 14 illustrates the measurement of pore and strut size from the optical microscopic image of the EBM produced dodecahedral lattice structure.

The μ -CT scan (BRUKER SKYCAM 1173, Belgium) was implemented to determine any stochastic defects and to demonstrate the inner construction of the struts in the lattice cube. The Skyscan 1173 offers high-energy μ -CT imaging for large,

dense, and low-density objects with improved stability of the focal spot position. This imaging technique visualizes the three-dimensional internal structure in a non-destructive way (without physical cutting). The accelerating source voltage used in this study was 120 kV along with an image pixel size of 12.03 μm . A high resolution of the X-ray beam with a focused spot size of 5 μm was concentrated on the lattice cube. Each 512×512 bitmap row of 2D slice image was collected as output data. The μ -CT scan outcomes of the internal lattice characterization are presented in Fig. 15.

To study the strength of the EBM-produced dodecahedral lattice cubes, an axial compressive test was also performed. The compressive strength of the EBM-produced cubes was analyzed using a 3385 H Instron universal tester (Instron, Massachusetts, United States) attached with a load cell of 100 KN and at a crosshead travel speed of 1 mm/min.

Fig. 14 Measurement of pore and strut size from the optical microscopic image of the dodecahedral structure

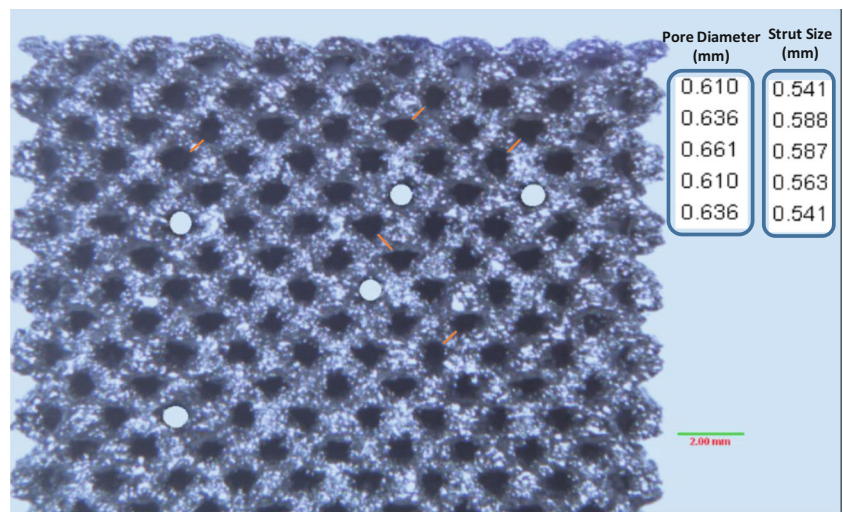
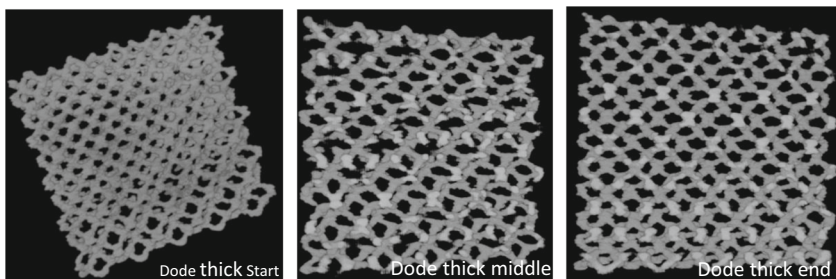


Fig. 15 Micro-CT scan images representing cross-sectional views of the dode thick lattice structure



2.5 Cost analysis

A comprehensive cost model was established to investigate the economics of fabricating the proposed design using EBM technology. Due to the additive fabrication of EBM parts, less material is wasted, which in turn, reduce the material cost and also the manufacturing time [46]. The EBM machine run time is the main cost-driving factor when compared to data preparation and energy consumption. For the last decade, the capital cost of additive manufacturing machines has fallen dramatically. Certainly, the machine cost and material cost are also likely to drop significantly owing to more competition in the market. Multiple parts can be fabricated in EBM under a single build. In addition to the benefits of costs, energy, and sustainability, AM properties and performance are important factors in assessing the suitability of this technology. The EBM technology can produce parts with properties exceeding those manufactured by traditional process [47]. The cost model for EBM technology can be defined as follows:

$$\text{Cost Model } C_{\text{Build}} = \left[(C_{\text{Indirect}} \times T_{\text{Build}}) + (M_{\text{Part}} \times C_{\text{Raw}}) + (E_{\text{Build}} \times P_{\text{Energy}}) + (M_{\text{Hours}} \times C_{\text{Labor}}) \right]$$

Where,

- C_{Indirect} Indirect cost consisting of EBM ownership cost and maintenance cost, measured in \$/h,
- T_{Build} EBM total build time,
- M_{part} Mass of EBM-built parts including support structures,
- C_{Raw} Cost of the metal powder (Ti6Al4V ELI) measured in \$/g,
- E_{Build} Energy consumption for EBM-built part,
- P_{Energy} Price of energy consumption (electricity cost for EBM process), measured in \$/KWh,

- M_{Hours} Manual hours in the preparation of EBM-built parts,
- C_{Labor} Labor cost/ h

A comprehensive cost model spreadsheet for the fabrication of customized mandibular implant is presented in the table ST1 and their results were compared with the commercially available reconstruction plate produced through traditional techniques.

3 Results and discussions

The outcomes from the various tests have been presented in this section. For example, the elements Ti (Titanium), Al (Aluminum), and V (Vanadium) detected by EDS analysis on post fabrication were very close to the composition of the feedstock powder. Table 4 illustrates the EDS analysis results which indicated that the EBM-fabricated specimen did not differ much from the input powder.

The results from the laser diffraction technique on the powder indicated that the particle size distribution was intact with an original size distribution of 50 to 110 μm and a mean approximation of 75 μm. The SEM analysis revealed that the powder particle morphology remained to be spherical with no significant deviations in geometry and size from the manufacturer's data. The results of particle size distribution and powder morphology ensured that the powder had a constant flowability throughout the build process.

The strut thickness and pore diameter of the designed dode thick lattice structure were found to be 600 and 480 μm, respectively. The porosity percentage of the lattice structure was calculated using the volume parameter obtained from designed solid and dode thick lattice structure and measured as 75%. Several research studies have proved that titanium scaffold with a porosity of 75% and pore diameter in the range of

Table 4. Chemical composition of the feedstock powder and EBM fabricated specimen (Wt%).

	Al (Aluminum)	V (Vanadium)	Ti (Titanium)
Feedstock powder	6.4	4.0	89.6
EBM Fabrication Specimen	6.24	3.89	89.87

Table 5 Comparison between experimental and theoretical values

Specimen	Strut thickness (μm)	Pore diameter (μm)
Design value	600	480
EBM-fabricated value	560	620
Difference in percentage	-7.14	22.5

200 to 620 μm provides excellent metabolic cell activity and cell migration [27, 48]. The pore size and porosity in our study were within the range considered optimal in the literature. The average strut thickness and pore diameter of the EBM-fabricated lattice structure were estimated to be 560 and 620 μm . Table 5 summarizes the difference in percentage between the design value and the EBM-fabricated value of struts and pores. The percentage difference was calculated based on the following equation:

$$\text{Percentage difference} = \frac{(\text{EBM fabricated value} - \text{Design value}) \times 100}{\text{EBM fabricated value}}$$

The difference between the design and EBM-fabricated values can be attributed to the EBM shrinkage factor on the size of the struts which in turn increased the pore diameter. Earlier studies have also proved similar strut and pore size deviation from CAD design and fabricated scaffolds [8, 49]. This difference in discrepancy was due to the EBM-built parameters such as beam speed, scan rate, and beam current which defined the shape of the struts [50]. A regular lattice structure with a repeated array of cells provides less difference between the fabricated and the design values when compared to structures with complex cell types [51]. Moreover, the microscopic image showed no differentiation in the interlayer and complete melting of the metal powder when investigated on the exterior face of the lattice cube. It pointed out good metallurgical bonding between the layers of the lattice structure during the fabrication process. This outcome is significant because the presence of voids between the layers reduces the strength of the finished part.

The interconnectivity is another important factor that determines the effectiveness of porosity [52]. Weak

interconnectivity between pores leads to cracks and fractures. Pore size and interconnectivity affects how much cells can penetrate and grow into the scaffold. A good interconnected pore channel supports the vascular system and enhances continuous bone development [53]. Furthermore, it is a usual practice to perform the blasting of the EBM-produced sample after each build to remove the semi-sintered powder attached to the specimen, due to which, there are high chances of breakage of the internal struts. Therefore, the $\mu\text{-CT}$ analysis was carried out to validate the interconnectivity and the porosity of the produced specimen. The outcome from this investigation demonstrated that the EBM-fabricated lattice structures exhibited strong interconnectivity between pores and possessed an uninterrupted network of interconnected channels.

The results from the axial compressive test are depicted in Fig. 16. It establishes the stress–strain relationship curve of the lattice cube with a maximum strength of 15 MPa. It was observed from the compression test that the deformation of the lattice cubes started from collapsing of the individual layers which were adjacent and the edge of the cube.

Earlier research studies reported that the maximum biting force in the mandibular region for healthy patients ranges from 15 to 4341 N, depending upon their age, gender, and measurement method [54, 55]. Hernandez et al. [56] achieved a compressive strength of 11.7 MPa for its EBM-fabricated lattice Ti6Al4V material whereas Jayanthi et al. [57] attained a mere 7 MPa with the same Ti6Al4V alloy. We achieved a higher peak strength of 15 MPa, allowing the implant to withstand greater load and simultaneously reducing the stress shielding at the surrounding bone. Besides, the bite force measurement studies revealed a significant increase in measurement on post-operation of mandible reconstruction from 30 to 66% over 6 weeks [58, 59]. The EBM-fabricated dode thick lattice plate will have a significant increase in biting force and can subsequently withstand higher stresses of about 30 to 60% after 6 weeks.

Based on the cost analysis as shown in Table 6, it can be inferred that EBM is an expensive process to produce one custom plate from a single EBM-built setup, but if we produce at least 15 plates in one build, the cost will dramatically reduce. Therefore, if the requirement is for producing customized implants for a large number of patients, then EBM is the

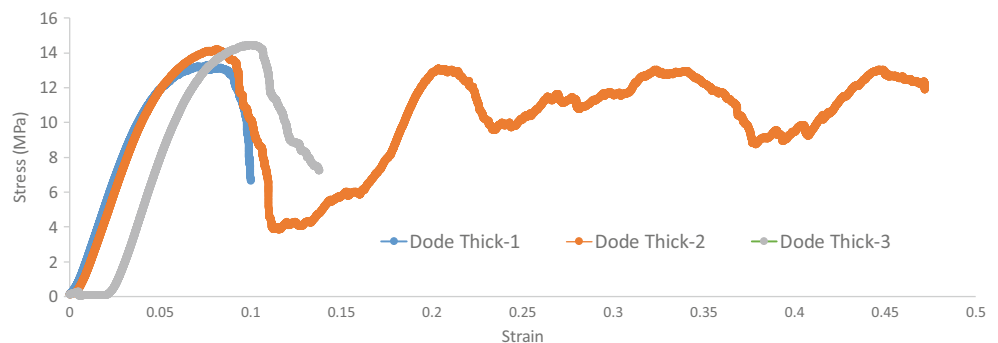
Fig. 16 Compressive stress–strain graph of dode thick structure

Table 6 Cost calculation for mandibular plates

Parts	Indirect cost	Build time	Part mass	Material cost	Energy consumption	Energy cost	Manual hours	Labor cost	Total cost	
Cost of 15 plates in one-build EBM setup	C_{indirect} (\$)	T_{build} (h)	M_{part} (g)	C_{raw} (\$/g)	E_{build} (KWh)	P_{energy} (\$/KWh)	M_{hours} (h)	C_{labor} (\$/h)	US dollars (\$)	
	29	16	140	0.22	112	0.085	3.5	5.33		
	$C_{\text{indirect}} \times T_{\text{build}}$ (\$29/h × 16 h) \$464		$M_{\text{part}} \times C_{\text{raw}}$ (140 g × \$0.22/g) \$30.80		$E_{\text{build}} \times P_{\text{energy}}$ (112 KWh × \$0.085/KWh) \$9.52		$M_{\text{hours}} \times C_{\text{labor}}$ (3.5 h × \$5.33/h) \$18.65			523
Cost of 1 plate from 15-plate EBM-build setup	29	3.5	9.33	0.22	24.5	0.085	3.5	5.33	35	
Single plate in one-build EBM setup	$C_{\text{indirect}} \times T_{\text{build}}$ (\$29/h × 3.5 h) \$101.5		$M_{\text{part}} \times C_{\text{raw}}$ (9.33 g × \$0.22/g) \$2.05		$E_{\text{build}} \times P_{\text{energy}}$ (24.5 KWh × \$0.085/KWh) \$2.08		$M_{\text{hours}} \times C_{\text{labor}}$ (3.5 h × \$5.33/h) \$18.65			124
Commercial single plate	\$101.5 + \$2.05 + \$2.08 + \$18.65 Reference [60, 61]								48–103	

right option economically. Besides, the commercially available reconstruction plates produced through conventional techniques is also a lengthy process with expensive mold designs. Besides, the commercial titanium plates are not patient-specific and come in standard shapes and sizes. The surgeons before surgery spend a considerable amount of time (1 to 2 h) to custom fit the commercial plate onto the patient bone contour. In the case of producing a customized plate using a traditional technique such as casting [62] and wrought techniques [63], the cost of each plate will be too high due to its expensive mold design for each patient.

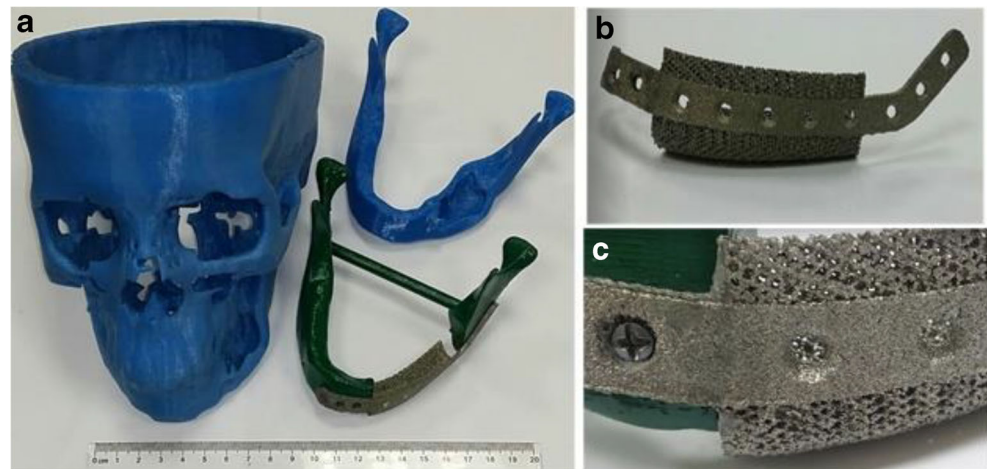
The cost of each commercially available titanium reconstruction plate (non-customized) is in the range of \$48 to \$103 depending upon the supplier [60, 61]. In contrast, the cost of the EBM-fabricated implant is \$35, when at least 15 customized implants are fabricated. Previous studies have indicated a cost reduction of 35% for customized implants produced through the EBM process when compared to traditional techniques [64]. In the case of fabrication of a single customized plate in one EBM build, the cost is much higher reaching \$124.28.

Finally, the EBM-fabricated defect-free titanium reconstruction plate was assembled on the polymer mandibular model produced through fused deposition modeling to evaluate its final fitting before surgery as shown in Fig. 17. On successful fitting assessment, the titanium lattice plate was washed with acetone, distilled water, and dehydrated alcohol before sterilization to remove the biological contamination. Gamma irradiation and oxygen plasma are some of the sterilization processes which can also be used to free the reconstruction plate from all viable microorganisms [42].

4 Conclusion

The progress in engineering technologies, such as state-of-the-art image acquisition systems, advanced modeling software, and additive manufacturing has uniquely changed the way implants are designed and fabricated for the medical industry. However, there are inconsistencies and gaps, due to lack of studies concerning the restoration of large and complicated mandibular defects, inadequate applications involving smooth integration of various design and manufacturing phases, unsatisfactory quality validation procedures, as well as insufficient lattice structures and their performance investigations. Therefore, to address some of these issues, a methodology has been introduced to achieve a robust and reliable additively manufactured porous implant for large mandibular defects. The primary objective of this study was the seamless integration of the different phases for mandible rehabilitation. It intended on automating the procedure of acquiring the tailor-made scaffold implant through design, analysis, assessment, and fabrication of the mandibular defect. The primary outcome of this study

Fig. 17 **a** Polymer mandibular models and EB-fabricated titanium lattice plate, **b** titanium lattice plate after support removal, and **c** close-up view of the lattice implant attached to the polymer model



was a comprehensive roadmap required for the design and fabrication of customized mandible implants.

A patient-specific plate was designed and fused with a mesh structure to support the building of surrounding bones. The customized lattice implant for mandibular reconstruction was designed from the patient's CT scan data and simulated for biomechanical analysis under chewing conditions and fabricated using EBM. The simulation of the designed reconstruction plate resulted in a maximum of 214.77 MPa of Von Mises stress which was significantly below the yield strength (800 MPa) of the material (Ti6Al4V ELI) used for the implant study. Moreover, the EDS and a μ -CT scan confirmed that the EBM-fabricated lattice reconstruction plate possessed a uniform network of channels that were free from cracks and impurities. The EBM-fabricated lattice reconstruction plate also fitted closely onto the mandibular bone, providing rigidity and flexibility to the implant. The cost analysis clearly showed that the initial cost of EBM system acquisition was considerably higher but the cost/part reduced significantly thus making it more competitive when a large number of reconstruction plates were fabricated. The additively fabricated implant prototypes help the surgeons to plan, navigate, and rehearse the surgical corridor preoperatively, thereby easing the difficulty and lowering the operation time of complex surgical cases.

The outcomes asserted EBM-fabricated customized lattice plates is a potential bone substitute in large mandibular defects. This research is especially useful because it provides a description of each step in each phase to guide future studies. Moreover, this approach can also reduce the number of revisions and surgery time as well as provide a faster healing time with good implant tissue in-growth. However, this approach needs collaborative disciplines so that ideal practices can be synergized to promote and nurture innovation in this field of medical implants. In future work, this proposed research approach can also be assimilated in other bone defects where reconstruction plates are needed.

Acknowledgments The authors extend their appreciation to the Deanship of Scientific Research at King Saud University for funding this work through Research group no, RG-1440-034.

Compliance with ethical standards

Conflict of interest The authors have no conflict of interest to declare.

References

1. Carlsen A, Marcussen M (2016) Spontaneous fractures of the mandible concept & treatment strategy. *Med Oral Patol Oral Cir Bucal* 21(1):e88–e94
2. Dabrowski B, Swieszkowski W, Godlinski D, Kurzydowski KJ (2010) Highly porous titanium scaffolds for orthopaedic applications. *J Biomed Mater Res B Appl Biomater* 95(1):53–61
3. Jiang J, Xu X, Stringer J (2018) Support structures for additive manufacturing: a review. *J Manuf Mater Process* 2(4):64
4. Jiang J, Xu X, Stringer J (2019) Optimisation of multi-part production in additive manufacturing for reducing support waste. *Virtual Phys Prototyp* 14(3):219–228
5. Ford S, Despeisse M (2016) Additive manufacturing and sustainability: an exploratory study of the advantages and challenges. *J Clean Prod* 137:1573–1587
6. Chua CK, Wong CH, Yeong WY (2017) Standards, quality control, and measurement sciences in 3D printing and additive manufacturing. Academic Press
7. Otsuki B, Takemoto M, Fujibayashi S, Neo M, Kokubo T, Nakamura T (2006) Pore throat size and connectivity determine bone and tissue ingrowth into porous implants: three-dimensional micro-CT based structural analyses of porous bioactive titanium implants. *Biomaterials*. 27:5892–5900
8. Onal E, Frith J, Jurg M, Wu X, Molotnikov A (2018) Mechanical properties and in vitro behavior of additively manufactured and functionally graded Ti6Al4V porous scaffolds. *Metals* 8(4):200
9. Li X, Luo Y, Wang C, Zhang W, Li Y (2012) Fabrication and in vivo evaluation of Ti6Al4V implants with controlled porous structure and complex shape. *Front Mech Eng* 7:66–71
10. Parthasarathy J (2013) 3D modeling, custom implants and its future perspectives in craniofacial surgery. *Ann Maxillofac Surg* 4(1):9

11. Erk KA, Dunand DC, Shull KR (2008) Titanium with controllable pore fractions by thermoreversible gelcasting of TiH₂. *Acta Mater* 56(18):5147–5157
12. Li J, Habibovic P, Vandendoel M, Wilson C, Dewijn J, Vanblitterswijk C, Degroot K (2007) Bone ingrowth in porous titanium implants produced by 3D fiber deposition. *Biomaterials* 28(18):2810–2820
13. Anurag R, Kumar SR, Joshi KK, Sahoo AK, Das RK (2018) Machining of Ti-6Al-4V ELI alloy: a brief review. *IOP Conf Ser Mater Sci Eng* 390:012112
14. Materialise Mimics, <https://www.materialise.com/en/medical/software/mimics>
15. Platform: Integrated Simulation System | ANSYS, <https://www.ansys.com/products/platform>
16. LightSpeed VCT, <https://www.gehealthcare.com/courses/lightspeed-vct>
17. Moiduddin K, Anwar S, Ahmed N, Ashfaq M, Al-Ahmari A (2017) Computer assisted design and analysis of customized porous plate for mandibular reconstruction. *IRBM* 38(2):78–89
18. Moiduddin K, Darwish S, Al-Ahmari A, ElWatidy S, Mohammad A, Ameen W (2017) Structural and mechanical characterization of custom design cranial implant created using additive manufacturing. *Electron J Biotechnol* 29:22–31
19. Alassaf MH, Li W, Joshi AS, Hahn JK (2014) Computer-based planning system for mandibular reconstruction. *Stud Health Technol Inform* 196:6–10
20. Mohammadhosseini A, Masood SH, Fraser D, Jahedi M, Gulizia S (2017) Flexural behaviour of titanium cellular structures produced by Electron beam melting. *Mater Today Proc* 4(8):8260–8268
21. Yang Y, Wang G, Liang H, Gao C, Peng S, Shen L, Shuai C (2018) Additive manufacturing of bone scaffolds. *Int J Bioprint* 5(1)
22. Cansizoglu O, Harrysson O, Cormier D, West H, Mahale T (2008) Properties of Ti-6Al-4V non-stochastic lattice structures fabricated via electron beam melting. *Mater Sci Eng A* 492:468–474
23. Horn TJ, Harrysson OLA, Marcellin-Little DJ, West HA, Lascelles BDX, Aman R (2014) Flexural properties of Ti6Al4V rhombic dodecahedron open cellular structures fabricated with electron beam melting. *Addit Manuf* 1–4:2–11
24. Harrysson OL, Cansizoglu O, Marcellin-Little DJ, Cormier DR, West HA II (2008) Direct metal fabrication of titanium implants with tailored materials and mechanical properties using electron beam melting technology. *Mater Sci Eng C* 28:366–373
25. Bragdon CR, Jasty M, Greene M, Rubash HE, Harris WH (2004) Biologic fixation of total hip implants: insights gained from a series of canine studies. *J Bone Joint Surg* 86:105–117
26. Mour M, Das D, Winkler T, Hoenig E, Mielke G, Morlock MM, Schilling AF (2010) Advances in porous biomaterials for dental and orthopaedic applications. *Materials* 3(5):2947–2974
27. Markhoff J, Wieding J, Weissmann V, Pasold J, Jonitz-Heincke A, Bader R (2015) Influence of different three-dimensional open porous titanium scaffold designs on human osteoblasts behavior in static and dynamic cell investigations. *Materials* 8(8):5490–5507
28. S. Materialise: Structures module, <https://www.materialise.com/en/software/magics/modules/structures-module>
29. Atilgan S, Erol B, Yardimedden A, Yaman F, Ucan MC, Gunes N, Atalay Y, Kose I (2010) A three dimensional analysis of reconstruction plates used in different mandibular defects. *Biotechnol Biotechnol Equip* 24(2):1893–1896
30. Vajgel A, Camargo IB, Willmersdorf RB, de Melo TM, Laureano Filho JR, Vasconcellos RJ (2013) Comparative finite element analysis of the biomechanical stability of 2.0 fixation plates in atrophic mandibular fractures. *J Oral Maxillofac Surg* 71(2):335–342
31. Silva GC, Mendonça JA, Lopes LR, Landre J (2010) Stress patterns on implants in prostheses supported by four or six implants: a three-dimensional finite element analysis. *Int J Oral Maxillofac Implants* 25(2):239–246
32. Arcam: Ti6Al4V ELI titanium alloy. <http://www.arcam.com/wp-content/uploads/Arcam-Ti6Al4V-ELI-Titanium-Alloy.pdf>
33. Martin B (1993) Aging and strength of bone as a structural material. *Calcif Tissue Int* 53(1):S34–S40
34. Wang X, Puram S (2004) The toughness of cortical bone and its relationship with age. *Ann Biomed Eng* 32(1):123–135
35. Simonovics J, Bujtár P, Váradi K (2013) Effect of preloading on lower jaw implant. *Biomech, Hung*
36. Szucs A, Bujtár P, Sándor GKB, Barabás J (2010) Finite element analysis of the human mandible to assess the effect of removing an impacted third molar. *J Can Dent Assoc* 76:a72
37. Meriç G, Erkmen E, Kurt A, Eser A, Ozden AU (2012) Biomechanical comparison of two different collar structured implants supporting 3-unit fixed partial denture: a 3-D FEM study. *Acta Odontol Scand* 70(1):61–71
38. Canullo L, Pace F, Coelho P, Sciubba E, Voza I (2011) The influence of platform switching on the biomechanical aspects of the implant-abutment system. A three dimensional finite element study. *Med Oral Patol Oral Cir Bucal* 16(6):e852–e856
39. Narra N, Valášek J, Hannula M, Marcián P, Sándor GK, Hyttinen J, Wolff J (2014) Finite element analysis of customized reconstruction plates for mandibular continuity defect therapy. *J Biomech* 47(1):264–268
40. Yu Y, Zhu R, Zeng Z-L, Jia Y-W, Wu Z-R, Ren Y-L, Chen B, Ding Z-Q, Cheng L-M (2014) The strain at bone-implant interface determines the effect of spinopelvic reconstruction following total sacrectomy: a strain gauge analysis in various spinopelvic constructs. *PLoS ONE* 9(1)
41. Ning X, Wen Y, Xiao-Jian Y, Bin N, De-Yu C, Jian-Ru X, Lian-Shun J (2008) Anterior cervical locking plate-related complications; prevention and treatment recommendations. *Int Orthop* 32(5):649–655
42. Basciftci FA, Korkmaz HH, Üşümez S, Eraslan O (2008) Biomechanical evaluation of chin cup treatment with various force vectors. *Am J Orthod Dentofac Orthop* 134(6):773–781
43. Arcam A2 setting the standard for additive manufacturing, <http://www.arcam.com/wp-content/uploads/Arcam-A2.pdf>. Accessed: 12-Jul-2019
44. Salerno A, Maio ED, Iannace S, Netti PA (2011) Tailoring the pore structure of PCL scaffolds for tissue engineering prepared via gas foaming of multi-phase blends. *J Porous Mater* 19(2):181–188
45. Liu P, Chen G-F (2014) Porous materials, processing and applications. Elsevier
46. Geraedts J, Doubrovski E, Verlinden J (2012) Three views on additive manufacturing: business, research, and education. ResearchGate. TMCE, Karlsruhe
47. Facchini L, Magalini E, Robotti P, Molinari A (2009) Microstructure and mechanical properties of Ti-6Al-4V produced by electron beam melting of pre-alloyed powders. *Rapid Prototyp J* 15:171–178
48. Wysocki B, Idaszek J, Szlązak K, Strzelczyk K, Brynk T, Kurzydłowski KJ, Świąszkowski W (2016) Post processing and biological evaluation of the titanium scaffolds for bone tissue engineering. *Materials* 9(3)
49. Van Bael S, Kerckhofs G, Moesen M, Pyka G, Schrooten J, Kruth J-P (2011) Micro-CT-based improvement of geometrical and mechanical controllability of selective laser melted Ti6Al4V porous structures. *Mater Sci Eng A* 528:7423–7431
50. van Grunsven W, Hernandez-Nava E, Reilly GC, Goodall R (2014) Fabrication and mechanical characterisation of titanium lattices with graded porosity. *Metals* 4(3):401–409
51. Parthasarathy J, Starly B, Raman S (2011) A design for the additive manufacture of functionally graded porous structures with tailored mechanical properties for biomedical applications. *J Manuf Process* 13:160–170

52. Alvarez K, Nakajima H (2009) Metallic scaffolds for bone regeneration. *Materials*. 2(3):790–832
53. Li JP, Li SH, Van Blitterswijk CA, de Groot K (2005) A novel porous Ti6Al4V: characterization and cell attachment. *J Biomed Mater Res A* 73(2):223–233
54. Harada K, Watanabe M, Ohkura K, Enomoto S (2000) Measure of bite force and occlusal contact area before and after bilateral sagittal split ramus osteotomy of the mandible using a new pressure-sensitive device: a preliminary report. *J Oral Maxillofac Surg* 58(4):370–373; discussion 373–374
55. Madsen MJ, Haug RH (2006) A biomechanical comparison of 2 techniques for reconstructing atrophic edentulous mandible fractures. *J Oral Maxillofac Surg* 64(3):457–465
56. Hernández-Nava E, Smith CJ, Derguti F, Tammas-Williams S, Léonard F, Withers PJ, Todd I, Goodall R (2015) The effect of density and feature size on mechanical properties of isostructural metallic foams produced by additive manufacturing. *Acta Mater* 85:387–395
57. Parthasarathy J, Starly B, Raman S, Christensen A (2010) Mechanical evaluation of porous titanium (Ti6Al4V) structures with electron beam melting (EBM). *J Mech Behav Biomed Mater* 3(3):249–259
58. Gerlach KL, Schwarz A (2002) Bite forces in patients after treatment of mandibular angle fractures with miniplate osteosynthesis according to Champy. *Int J Oral Maxillofac Surg* 31(4):345–348
59. Kumar ST, Saraf S, Devi SP (2013) Evaluation of bite force after open reduction and internal fixation using microplates. *J Dent Tehran Iran* 10(5):466–477
60. Rustemeyer J, Melenberg A, Sari-Rieger A (2014) Costs incurred by applying computer-aided design/computer-aided manufacturing techniques for the reconstruction of maxillofacial defects. *J Craniomaxillofac Surg* 42(8):2049–2055
61. Gutwald R, Jaeger R, Lambers FM (2017) Customized mandibular reconstruction plates improve mechanical performance in a mandibular reconstruction model. *Comput Methods Biomech Biomed Eng* 20(4):426–435
62. M. Ashish: Process planning for the rapid machining of custom bone implants, (2011)
63. Hermawan H, Ramdan D, Djuansjah JRP (2011) Metals for biomedical applications. In: Fazel R (ed) *Biomedical engineering - from theory to applications*. InTech
64. Cronskär M, Bäckström M, Rännar L (2013) Production of customized hip stem prostheses – a comparison between conventional machining and electron beam melting (EBM). *Rapid Prototyp J* 19(5):365–372

Publisher's note Springer Nature remains neutral with regard to jurisdictional claims in published maps and institutional affiliations.